IEEE Access
Multidisciplinary | Rapid Review | Open Access Journal

Received 8 August 2024, accepted 25 August 2024, date of publication 3 September 2024, date of current version 11 September 2024.

*Digital Object Identifier 10.1109/ACCESS.2024.3454173*

RESEARCH ARTICLE

# Ground-Fault Recognition in Low-Voltage Ships Based on Variation Analysis of Phase-to-Ground Voltage and Neutral-Point Voltage

**KI-TAK RYU AND YUN-HYUNG LEE**
Korea Institute of Maritime and Fisheries Technology, Yeongdo-gu, Busan 49126, South Korea
Corresponding author: Yun-Hyung Lee (domse54@daum.net)

**ABSTRACT** Generally, ships use a three-phase power system with low-voltage and ungrounded systems to ensure continuous power supply. In these shipboard power systems, ground faults constitute approximately 95% of all faults. Most ground faults are caused by the single line-to-ground fault. Ground faults can cause blackouts, which significantly impact the safe operation of ships. Therefore, ship engineers should identify the ground-fault region for effective management and resolution. This study analyzes the variations in the phase-to-ground voltage and neutral-point voltage during a ground fault in a distribution network of an ungrounded low-voltage ship. We proposed a practical method for ship engineers to determine the ground-fault phase by measuring only the phase-to-ground voltages. To verify the applicability of the practical method to real ships, the line-to-ground capacitance was directly measured for a 225 V power system of a training ship. Moreover, we performed simulations based on the measurement data and analyzed the variation characteristics of the phase-to-ground voltage and neutral-point voltage during a single line-to-ground fault. Thus, ship engineers can use the simulation results and proposed table to accurately determine ground faults by measuring only the phase-to-ground voltages.

**INDEX TERMS** Ground fault, line-to-ground capacitance, neutral-point voltage, phase-to-ground voltage, ungrounded system.

## I. INTRODUCTION

The reliability of an electrical system is crucial in a distribution network [1]; therefore, various grid grounding systems, such as ungrounded, resistance-grounded, reactance-grounded, and solidly grounded systems, are applied. Generally, the reliability problems of most power systems originate from a single line-to-ground (SLG) fault.

Ungrounded and high-resistance grounded systems offer several advantages compared to low-resistance grounded or solidly grounded systems. In these systems, continuous operation can be achieved owing to the absence of a large, short-circuit current even during an SLG fault. Additionally, these systems can be easily controlled by separating the specific circuits after identifying the fault points, which can be removed when convenient [2], [3], [4]. Moreover, because the momentary voltage sag caused by the SLG fault is removed, the power quality improves and the zero-sequence harmonic current in the electronic power equipment decreases [5]. SLG faults increase the phase-to-ground voltage of healthy phases, damage cable insulation, and, in severe cases, cause wide-ranging damage or system blackouts [6], [7]. Furthermore, serious electric shocks may occur in the event of high-resistance faults (HRFs) [8].

Ground faults are common in mines, where most power systems are ungrounded or resistance-grounded to reduce ground-fault current, blackouts, and electric shocks [9], [10], [11], [12], [13]. Similar to the mining industry, ungrounded systems are used in ships to secure continuous power supply [14]. However, in ships, the occurrence of ground faults and their location cannot be easily determined. The detection of ground faults is challenging in the case of HRF because

The associate editor coordinating the review of this manuscript and approving it for publication was Qiang Li.

the variations in the neutral-point voltage (or zero-sequence voltage), phase-to-ground voltage, and ground-fault current are not large [15], [16], [17]. Moreover, ground faults occur frequently, accounting for approximately 95% of all electrical faults [18]. These can cause power outages and significantly affect the safe operation of ships, resulting in collisions and strandings. Therefore, the prompt and precise detection of faults in ships is critically important.

The diagnostic methods for SLG faults in conventional power distribution networks can be divided into steady-state signal analysis and transient signal analysis, as opposed to those for maritime applications. The former primarily utilizes power frequency and harmonic signals generated for fault analysis [19], [20]. Additionally, another method involves extracting the fifth harmonic zero-sequence current of each line and detecting the faulty line through correlation analysis [21]. However, this approach assumes that the grounding resistance remains constant. The latter method leverages the fact that the magnitude of the transient signals during a ground fault is significantly higher than that of the steady-state signals. Recently, diagnostic methods based on fault transient signals have become a focal point of research [22], [23]. However, these methods require complex equipment to measure zero-sequence transient current, the frequency of extracted signals, and the speed of the traveling waves of the feeder, and are also prone to noise interference.

Meanwhile, with the development of data monitoring systems, the proposed data-driven approach performs fault diagnosis tasks by training and fitting on historical data from the distribution network [24], [25], [26]. It requires no prior knowledge and is suitable for complex distribution networks that are difficult to model. While these methods exhibit good classification capabilities, they consume significant memory and execution time when processing large volumes of data. Additionally, they are susceptible to local minima and overfitting.

The distribution system of the low-voltage ships considered in this study differs significantly from large-scale land-based distribution networks, as it is compact, independent, and employs an ungrounded system. Moreover, conventional SLG fault diagnosis methods are complex and require specialized equipment, which pose a significant challenge for ship engineers during operations. Owing to these factors, there is a paucity of research in which SLG fault diagnosis methods are directly applied to operational ships and where rigorous comparative analyses have been carried out based on established techniques.

Therefore, this study proposes an innovative SLG fault diagnosis method for practical application in ships operating based on low-voltage ungrounded systems to identify ground faults by measuring the phase-to-ground voltage. This is highly practical as it enables engineers to identify ground faults by measuring phase-to-ground voltages, offering greater availability compared to conventional methods. This approach utilizes the unique characteristics of ship power distribution systems, which are attributed to the asymmetry of line-to-ground capacitances and varying resistance values of ground-fault points. Specifically, in an SLG fault, the neutral-point voltage (or zero-sequence voltage) follows specific rules [27], which can be identified by variations in the phase-to-ground voltages of the three-phase system according to the resistance values of the ground-fault points.

Accordingly, we mathematically modeled the phase-to-ground voltage and neutral-point voltage in cases of ground faults in ships. Thereafter, the variation characteristics of these voltages were identified from the normal condition to the complete-ground fault. The range of voltage variations was divided into three segments for convenience of analysis. The line-to-ground capacitances were directly measured for a 225 V (rated voltage) electrical system of a training ship to verify the applicability of this method to real ships. Based on these measurements, simulations were performed using MATLAB® 2016a (MathWorks, Inc., Natick, Massachusetts, USA) for both symmetry and asymmetry of the line-to-ground capacitance. Subsequently, the variation characteristics of the phase-to-ground voltage and neutral-point voltage were analyzed via simulations. Furthermore, we propose a highly practical methodology that can be generalized and extended to arbitrary ships.

## II. MATHEMATICAL MODELING OF PHASE-TO-GROUND VOLTAGE AND NEUTRAL-POINT VOLTAGE IN THE EVENT OF GROUND FAULT

A schematic of an SLG (a-phase) fault in low-voltage ships with ungrounded systems is illustrated in Fig. 1.

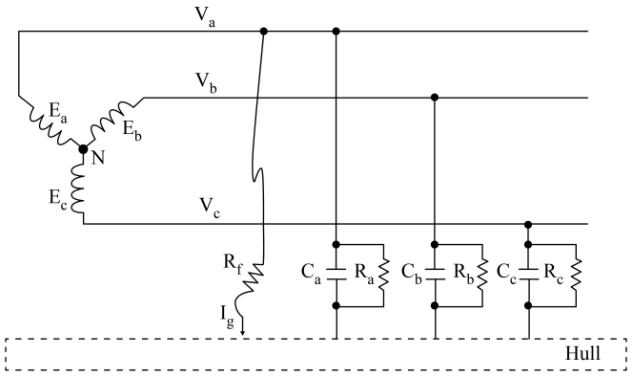


**FIGURE 1.** Ungrounded system with SLG fault in ships.

In Fig. 1, $N$ denotes the neutral point of the generator power source; $E_a$, $E_b$, and $E_c$ represent the phase voltages of the generator; $V_a$, $V_b$, and $V_c$ represent the phase-to-ground voltages; $C_a$, $C_b$, and $C_c$ indicate the line-to-ground capacitances; $R_f$ denotes the insulation resistance at the ground-fault points; and $R_a$, $R_b$, and $R_c$ represent the leakage resistances. In this study, we assumed these resistances to be equal for simplicity.

### A. NEUTRAL-POINT VOLTAGE DURING A-PHASE GROUND FAULT

As $E_a$, $E_b$, and $E_c$ have the same values, the neutral-point voltage in Fig. 1 is expressed as:

$$V_n = V_a - E_a = V_b - E_b = V_c - E_c. \tag{1}$$

The sum of the ground-fault currents that flow through the hull shown in Fig. 1 is expressed as follows:

$$V_a(\frac{1}{R} + j\omega C_a + \frac{1}{R_f}) + V_b(\frac{1}{R} + j\omega C_b) + V_c(\frac{1}{R} + j\omega C_c) = 0 \tag{2}$$

On substituting (1) into (2), the neutral-point voltage $V_{na}$ during an a-phase ground fault can be obtained as follows:

$$\begin{aligned} V_{na} &= -\frac{j\omega\,(C_aE_a + C_bE_b + C_cE_c) + \frac{E_a}{R_f}}{j\omega\sum C + \frac{3}{R} + \frac{1}{R_f}} \\ &= -\frac{j\frac{C_a+\boldsymbol{a}^2C_b+\boldsymbol{a}C_c}{\sum C} + \frac{1}{\omega\sum CR_f}}{j + \frac{1}{\omega\sum C}\left(\frac{3}{R} + \frac{1}{R_f}\right)}E_a \end{aligned} \tag{3}$$

where $\sum C = C_a + C_b + C_c$ and $\mathbf{a}$ indicates the vector operator $e^{-j\frac{2}{3}\pi}$.

Furthermore, if a ground fault occurs in the b-phase, $\frac{E_a}{R_f}$ in the numerator of (3) can be replaced with $\frac{E_b}{R_f}$, and the following equation is obtained.

$$V_{nb} = -\frac{j\frac{C_a+\boldsymbol{a}^2C_b+\boldsymbol{a}C_c}{\sum C} + \boldsymbol{a}^2\frac{1}{\omega\sum CR_f}}{j + \frac{1}{\omega\sum C}(\frac{3}{R} + \frac{1}{R_f})}E_a. \tag{4}$$

A ground fault that occurs in the c-phase can be interpreted similarly and $V_{nc}$ can be presented as follows:

$$V_{nc} = -\frac{j\frac{C_a+\boldsymbol{a}^2C_b+\boldsymbol{a}C_c}{\sum C} + \boldsymbol{a}\frac{1}{\omega\sum CR_f}}{j + \frac{1}{\omega\sum C}(\frac{3}{R} + \frac{1}{R_f})}E_a. \tag{5}$$

Additionally, the asymmetry ratio $r_a$ indicates the imbalance of the power distribution system and can be defined as follows:

$$r_a = \frac{C_a + \boldsymbol{a}^2C_b + \boldsymbol{a}C_c}{\sum C} = r_a\angle\alpha. \tag{6}$$

Theoretically, the maximum magnitude of $r_a$ is 5% in a pure overhead line, 0.5% in a pure cable line, and 1.5% in a mixed line [28].

Upon substituting (6) into (3), $V_n$ in the no-fault condition is expressed as

$$V_{n0} = -\frac{jr_acos\alpha - r_asin\alpha}{j}E_a = -r_a\,(cos\alpha + jsin\alpha)\,E_a. \tag{7}$$

According to (7), if the line-to-ground capacitances are symmetric in the no-fault condition, the initial point of $V_n$ is located at the origin. However, if the line-to-ground capacitances are asymmetric, the initial point of $V_n$ is located in a circle centered at the origin with radius $r_a$ and angle $\alpha$. If an a-phase ground fault occurs at this point; for example, from HRF to complete-ground fault, the trajectory of the neutral-point voltage is counterclockwise along a semicircular arc and is finally located at $-E_a$, as shown in Fig. 2. Furthermore, if a ground fault occurs in the b- or c-phase, the voltage trajectory is of a similar pattern and is finally located at $-E_b$ or $-E_c$, respectively.

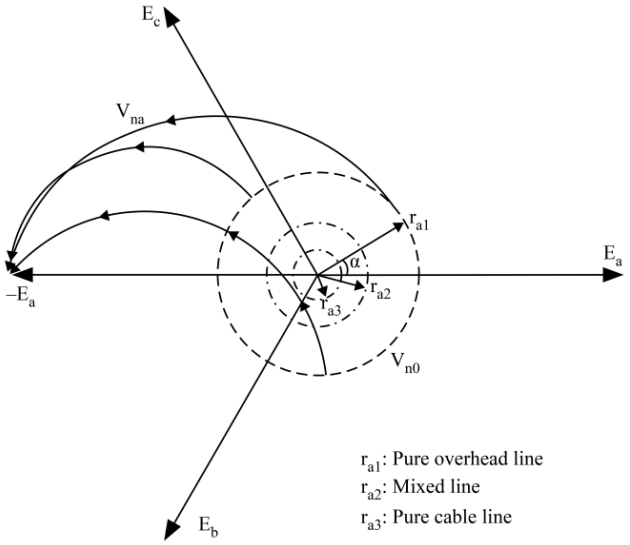


**FIGURE 2.** Trajectory of neutral-point voltage considering asymmetric line-to-ground capacitances during an a-phase ground fault.

### B. PHASE-TO-GROUND VOLTAGE DURING A-PHASE GROUND FAULT

During an a-phase ground fault, $V_a$(or $V_b$ or $V_c$) is calculated as the sum of $E_a$(or $E_b$ *or* $E_c$) and $V_{na}$, which can be expressed considering $r_a$ as follows:

$$V_a = E_a + V_{na} = (1 - \frac{jr_a + \frac{1}{\omega\sum CR_f}}{j + \frac{1}{\omega\sum C}(\frac{3}{R} + \frac{1}{R_f})}), \tag{8}$$

$$V_b = E_b + V_{na} = (\boldsymbol{a}^2 - \frac{jr_a + \frac{1}{\omega\sum CR_f}}{j + \frac{1}{\omega\sum C}(\frac{3}{R} + \frac{1}{R_f})})E_a, \tag{9}$$

$$V_c = E_c + V_{na} = (\boldsymbol{a} - \frac{jr_a + \frac{1}{\omega\sum CR_f}}{j + \frac{1}{\omega\sum C}(\frac{3}{R} + \frac{1}{R_f})})E_a. \tag{10}$$

## III. VARIATION CHARACTERISTICS OF PHASE-TO-GROUND VOLTAGE AND NEUTRAL-POINT VOLTAGE DURING AN SLG FAULT

To identify the SLG fault point, the variations in the magnitudes and phase angles of $V_a$(or $V_b$ or $V_c$) and $V_n$ were analyzed during the gradual decrease in $R_f$. The gradual decrease in $R_f$ can be considered as a decrease in insulation resistance owing to the aging of the power distribution system. Consequently, the noteworthy characteristics based on

the decrease in $R_f$ were examined, as discussed herein. Furthermore, the asymmetry of the line-to-ground capacitance was considered to include the characteristics of the actual power distribution systems.

### A. SYMMETRIC LINE-TO-GROUND CAPACITANCE

In this section, we examine the case in which the a-phase is grounded in a power distribution network considering a symmetric line-to-ground capacitance. Accordingly, if the resistance at the ground-fault point varies from $\infty$ (normal condition) to 0 (complete ground-fault condition), $V_n$ moves counterclockwise along a semicircle from the origin and is finally located at $-E_a$, as depicted in Fig. 3. Moreover, because $V_a = E_a + V_n$, as given in (1), the trajectory of $V_a$ has a pattern similar to that of $V_n$ as $R_f$ gradually decreases. The trajectories of $V_b$ and $V_c$ are similar to that of $V_a$ for the same reason.

In an ungrounded system, the variations in $V_a$(or $V_b$ or $V_c$) and $V_n$ are not significantly influenced by the magnitude of the line-to-ground capacitance [29].

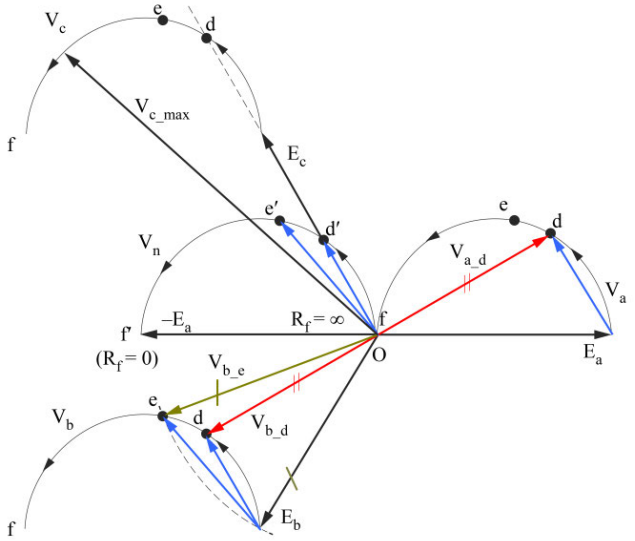


**FIGURE 3.** Vector diagram of phase-to-ground voltage and neutral-point voltage during an a-phase ground fault.

The trajectory of $V_n$ during the gradual decrease in $R_f$, as shown in Fig. 3, can be divided into three segments.

First, section O–d′ corresponds to the range from the no-fault condition to an HRF condition. The variations in the magnitudes of the phase-to-ground voltages in this segment are described as follows.

The magnitude of $V_c$, which is the phase to ground voltage of the healthy phase c, is greater than that of the phase voltage $E_c$. Additionally, $V_b$ (the phase to ground voltage of another healthy phase) and $V_a$ are less than the phase voltages $E_b$ and $E_a$, respectively. In this segment, the phase-to-ground voltages have the following magnitude relationship: $V_b < V_a < V_c$. Moreover, the phase angles of $V_b$ and $V_c$ are smaller than those of $E_b$ and $E_c$, respectively, and only the phase angle of $V_a$ is greater than that of $E_a$. When $V_n$ is located at point d′, the magnitudes of $V_b$ and $V_a$ are equal and the difference in phase angles of the two voltages is 180°. In this segment, as only the phase angle of the faulty phase increases, the faulty phase can be identified by carefully examining the relationship between the phase angles.

Second, in segment d′ –e′, $R_f$ decreases, and the magnitude relationship is $V_a < V_b$. Similar to that in segment O–d′, only the magnitude of $V_c$ is greater than $E_c$, whereas $V_b$ and $V_a$ are less than $E_b$ and $E_a$, respectively. However, $V_b$ becomes greater than $V_a$ in this segment, and the relationship $V_a < V_b < V_c$ is established. If $V_n$ originates from point e′, the magnitudes of $V_b$ and $E_b$ are equal. The relationship among the phase angles of these voltages can be described as follows: the phase angles of $V_c$ and $V_a$ surpass those of $E_c$ and $E_a$, and that of $V_b$ diminishes in comparison to that of $E_b$.

Third, in the segment e′–f′, $R_f$ gradually approaches zero, $V_a$ decreases continuously, and the magnitude of $V_b$ surpasses that of $E_b$. Moreover, $V_c$ continuously increases to become greater than $E_c$, and ultimately, becomes equal to the line-to-line voltage after passing through the maximum value of $V_{c\_max}$. The magnitude relationship of $V_a < V_b < V_c$ is maintained in this segment, similar to that observed in segment d′ –e′. Moreover, the phase angles of $V_c$ and $V_a$ exceed those of $E_c$ and $E_a$, respectively, whereas the phase angle of $V_b$ is reduced in comparison to that of $E_b$.

As discussed above, the variations in the phase-to-ground voltages compared to those of their phase voltages illustrated in Fig. 3 are summarized in Table 1.

**TABLE 1.** Variations of phase-to-ground voltages compared to those of phase voltages during an a-phase ground fault.

| Section | Magnitude | Phase angle |
|---|---|---|
| O–d′ | $V_a\downarrow, V_b\downarrow, V_c\uparrow$ $(V_b < V_a < V_c)$ | $\angle V_a\uparrow, \angle V_b\downarrow, \angle V_c\downarrow$ |
| d′–e′ | $V_a\downarrow, V_b\downarrow, V_c\uparrow$ $(V_a < V_b < V_c)$ | $\angle V_a\uparrow, \angle V_b\downarrow, \angle V_c\uparrow$ |
| e′–f′ | $V_a\downarrow, V_b\uparrow, V_c\uparrow$ $(V_a < V_b < V_c)$ | $\angle V_a\uparrow, \angle V_b\downarrow, \angle V_c\uparrow$ |

With further understanding, these characteristics can enable ship engineers to accurately recognize and identify the faulty phase during an HRF.

### B. ASYMMETRIC LINE-TO-GROUND CAPACITANCE

The distribution network systems of ships comprise a large portion of cables and small portion of overhead lines, such as bus-bars. Even if the cables and overhead lines in power distribution systems are wired with identical specifications, the asymmetry ratio shows a certain deviation in each case. If distribution systems operate normally, the initial point of

$V_n$ is located on a circle centered at the origin with a radius of $r_a$, as indicated in Fig. 2 and (7). As explained above, the maximum asymmetry ratio of line-to-ground capacitance for the distribution network system of ships is comprised of mixed lines; therefore, it can be considered 1.5%. In these systems, the initial point of $V_n$ is positioned inside a circle having a radius equal to 1.5% of the phase voltage.

## IV. SIMULATION RESULTS AND ANALYSIS

Before simulations, it must be checked whether a ground fault has occurred in the distribution network of the ship.

As a criterion to assess a ground fault, we applied the results of an existing study [30], which revealed that when a ground fault occurs, the neutral-point voltage exceeds 15% of the phase voltage. Therefore, the neutral-point voltage should be measured first and compared with the magnitude of the phase voltage.

Subsequently, a simulation was conducted considering both the symmetry and asymmetry of the line-to-ground capacitance. If it was assumed to be symmetric, $C_a$, $C_b$, and $C_c$ measured on board were averaged; if it was assumed to be asymmetric, the measured values were used as they were.

Therefore, a simulation that analyzes the magnitudes and phase angles of phase-to-ground voltages and neutral-point voltages enables ship engineers to identify and verify the ground fault. To this end, a simulation was applied to a training ship "H," which was operated by Korea Institute of Maritime and Fisheries Technology (KIMFT) to verify the validity and effectiveness of our method. The general specifications of the training ship are listed in Table 2, and the ship image is presented in Fig. 4.

**TABLE 2. General specifications of training ship "H".**

| | Training ship general data |
|---|---|
| Gross tonnage | 4,108 tons |
| Main engine power | 3,089 kW |
| Max. speed | 17.0 knots |
| Length | 87.55 m |
| Breadth | 16.0 m |
| Height | 10.0 m |
| Maximum number of people on board | 180 persons |

The overall distribution network of the training ship "H" is presented in Fig. 5. In particular, section "K" was selected as the distribution network analyzed in the simulation, which is a 225 V electrical circuit through the 450/225 V transformer. In accordance with IEC standards, the phase angle displacement of this transformer is denoted by Dd0, which is widely used in maritime applications.

The line-to-ground capacitances for the three phases in section "K" were measured using an LCR meter. Notably, the "K" section was disconnected from the electrical system to measure the line-to-ground capacitances, and the LCR-6100 (GW Instek, New Taipei City, Taiwan) was used as the LCR meter. More specifically, the parameter "Func" was set to Cp-D, "Freq" to 1.0 kHz, "Level" to 1.0 V, "Range" to Auto, "Trig" to INT, and "Speed" to Slow.

**FIGURE 4. Exterior of a training ship "H".**

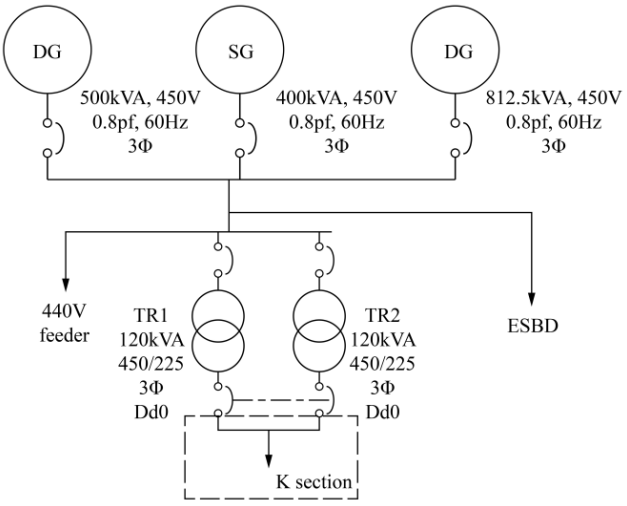


**FIGURE 5. Single-line diagram of the distribution system of the training ship "H".**

An example of the actual measurement in section "K" is depicted in Fig. 6, and the measured values for each phase are listed in Table 3. The results show that while the values for the three phases are nearly identical, minor differences are present. This suggests that the line-to-ground capacitance inherently contains a degree of asymmetry.

**TABLE 3. Measured values in the "K" section.**

| Phases | Phase-to-ground capacitance (μF) | Dissipation factor (D) |
|---|---|---|
| a | 2.66451 | 0.03195 |
| b | 2.70308 | 0.02986 |
| c | 2.66257 | 0.03286 |

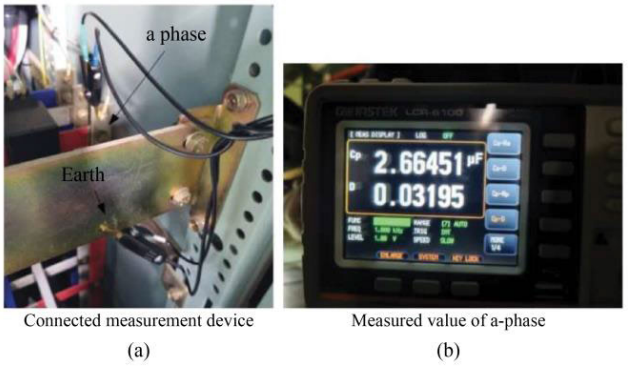


**FIGURE 6.** Measuring phase-to-ground capacitance of a-phase.

### A. SYMMETRIC CASE OF LINE-TO-GROUND CAPACITANCE

As described above, the symmetric case uses the average values listed in Table 3. The calculated average value of 2.6767 $\mu$F (This means that $C_a = C_b = C_c$) and phase voltage of 129.9 V ($225/\sqrt{3}$ V) were considered in the simulation.

For a decreasing a-phase insulation resistance $R_f$, the variations in $V_a$, $V_b$, and $V_c$, and that in $V_n$ are plotted in Figs. 7a and 7b, respectively.

As discussed earlier, the ground fault occurred at $V_n = 19.5$ V, which is 15% of the phase voltage of 129.9 V.

At this instant, $R_f = 2{,}175\ \Omega$, and $V_a = 128.4\ \angle 8.6°$ V, $V_b = 115.3\ \angle -126°$ V, and $V_c = 148.2\ \angle 117.2°$ V.

In particular, $V_c > E_c$ and $V_a > V_b$ in the section where $572\Omega \leq R_f < 2{,}175\Omega$, and $V_b$ gradually decreased within a small range, and its minimum value is $V_b = 106.8\ \angle -139.0°$ V for $R_f = 888\ \Omega$. The phase angles of $V_b$ and $V_c$ decreased more within a narrow range than their phase voltages, but the increase in the phase angle of $V_a$ was slightly greater than that of its phase voltage. The point at which $R_f = 572\ \Omega$ corresponds to point d′ in Fig. 3, where $V_a = 112.5\ \angle 30°$ V, $V_b = 112.5\ \angle -150°$ V, $V_c = 194.8\ \angle 120°$ V, and $V_n = 64.9\ \angle 120°$ V. As observed at this point, the magnitudes of $V_a$ and $V_b$ were equal, the phase difference of these two voltages was 180°, and $V_n$ and $V_c$ had the same phase angle. Beyond d′, $V_a$ (for faulty phase) became the smallest, $V_b < E_b$, and $V_c > E_c$. Overall, the phase angle of $V_b$ decreased, and the phase angles of $V_c$ and $V_a$ increased continuously.

For $R_f = 381\ \Omega$, $V_a = 98.1\ \angle 40.9°$ V, $V_b = 129.9\ \angle -158.2°$ V, $V_c = 214\ \angle 124.3°$ V, and $V_n = 85\ \angle\ 130.9°$ V, corresponding to point e′ in Fig. 3 at which $V_b$ becomes equal to $E_b$. Thereafter, $V_a$ continuously decreased and $V_b$ increased monotonously to surpass $E_b$. Although $V_c$ increased beyond $E_c$, it ultimately emerged as the line-to-line voltage of 225 V after surpassing the maximum value of 236.7 V.

### B. ASYMMETRIC CASE OF LINE-TO-GROUND CAPACITANCE

As presented in Table 3, the three-phase line-to-ground capacitances in section "K" are asymmetric. The values

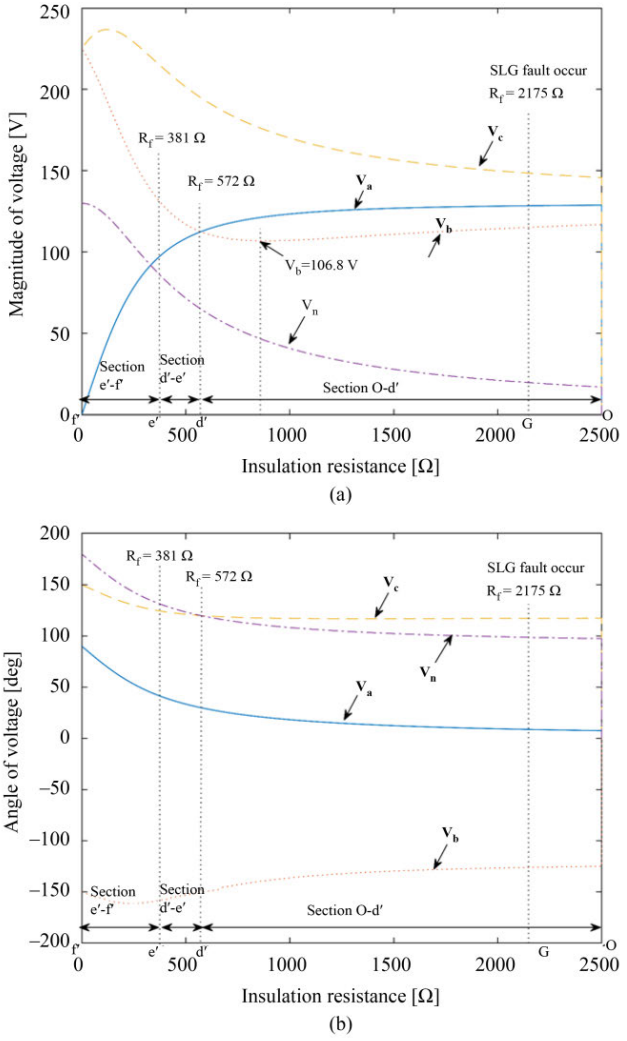


**FIGURE 7.** Variations in phase-to-ground voltage and neutral-point voltage for symmetrical network during a-phase ground fault.

show that $r_a$ was 0.0049 $\angle 117.5669°$ following (6), and the asymmetry ratio was 0.49%.

Fundamentally, the ship was wired mainly using cables, and overhead lines such as bus-bars were only partially used. For this reason, $r_a$ in section "K" almost approached the maximum asymmetry ratio of a pure cable line.

In the case of asymmetry, the variation characteristics of the phase-to-ground voltage and neutral-point voltage were examined by applying the values measured during the a-phase ground fault.

For a decreasing $R_f$, the variations in the magnitudes and phase angles of $V_a$, $V_b$, $V_c$, and $V_n$ obtained from the simulations are plotted in Fig. 8.

As noted earlier, the ground fault occurs at $V_n = 19.5$ V, which is 15% of the phase voltage (129.9 V). At this instant, $R_f = 2{,}242\ \Omega$, $V_a = 128.8\ \angle 8.6°$ V, $V_b = 115.0\ \angle -125.9°$ V, and $V_c = 148.1\ \angle 117.1°$ V.

When $R_f = 893\ \Omega$, $V_b$ exhibits the minimum value of $V_b = 106.4\ \angle -139.1°$ V. For $R_f = 567\ \Omega$ corresponding to

point d′ in Fig. 3, $V_a = 112.5\ \angle 30.4°$ V, $V_b = 112.5\ \angle -150.4°$ V, $V_c = 195.7\ \angle 120°$ V, and $V_n = 65.8\ \angle 120°$ V. Additionally, as $R_f$ decreases further to 381 Ω, corresponding to point e′ in Fig. 3, $V_a = 98.3\ \angle 41.1°$ V, $V_b = 129.9\ \angle -158.4°$ V, $V_c = 214.5\ \angle 124.2°$ V, and $V_n = 85.5\ \angle 130.7°$ V.

These results reveal that the pattern of voltage variation of the asymmetric case is not significantly different from that observed in the symmetric case.

### C. UNDER VARIATION OF ASYMMETRY RATIO ANGLE α

According to (7), the initial point of the neutral-point voltage under normal conditions is located at any point on a circle centered at the origin based on the value of $r_a$ and its angle $\alpha$. Consequently, an assessment of the changes in $r_a$ and angle $\alpha$ is necessary.

As described previously, the value of $r_a$ measured in section ''K'' was very close to the maximum asymmetry ratio of a pure cable line. To examine the influence of changes in $r_a$, the simulation is performed by setting $r_a$ to 1.5%, which is the maximum capacitance limit of the mixed line. This assumes that the asymmetry ratio increases with the distribution capacity of the ship. Moreover, $r_a$ is set to 1.5%, and the phase angle $\alpha$ is varied from 0°–350° in the intervals of 10° (36 intervals).

The variation characteristics of the phase-to-ground voltage and neutral-point voltage based on the phase angle ($\alpha$) of $r_a$ are depicted in Fig. 9. With this result, the 36 magnitudes and phases do not intersect with each other and display the same pattern as in Fig. 8. This implies that there is no influence on the variation tendency of the phase-to-ground voltage and neutral-point voltage even though $r_a$ and $\alpha$ change.

### D. OCCURRENCE OF GROUND FAULT IN b- OR c-PHASE

Based on the simulation results presented up to this point, the variation characteristics of the phase-to-ground voltage and neutral-point voltage could be identified based on the degree of the a-phase ground fault. However, in practice, a ground fault may occur in the b- or c-phase rather than a-phase. Therefore, this section examines the variation characteristics of the phase-to-ground voltage in b- and c-phases during the gradual decrease of $R_f$. Fig. 10 shows the phase-to-ground voltage based on the degree of the ground fault in the a-, b-, and c-phases, as discussed above. The variation characteristics are similar to those of the a-phase ground fault despite the difference in ground fault phases.

This implies that the ground fault can be generalized to the results of Fig. 8, regardless of the phase in which it occurs. In the following section, a practical method to determine the ground fault is proposed.

### E. PRACTICAL METHOD TO DETERMINE GROUND FAULT IN SHIPS

Ship engineers must speedily identify the occurrence of a ground fault, otherwise it can damage the generator or cause a two-phase short circuit.

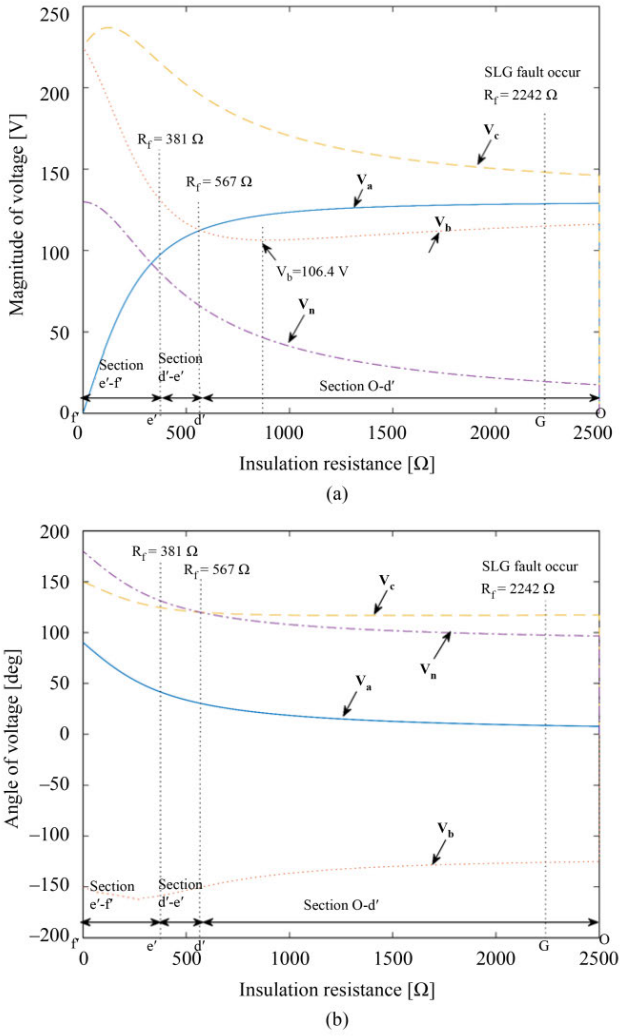


**FIGURE 8.** Variations in phase-to-ground voltage and neutral-point voltage for an asymmetrical network during a-phase ground fault.

The variation characteristics of phase-to-ground voltages during an arbitrary phase ground fault in section ''K'' of the training ship ''H'' are depicted in Figs. 11–13 (refer to the blue line).

The ranges of the phase-to-ground voltage, when an SLG fault occurs in a faulty phase, are shown in Fig. 11. This voltage gradually decreased to zero eventually, corresponding to a complete ground-fault condition. In Section G–d′, Point G represents the SLG fault point, and the voltage ranged between a minimum of 112.5 V and a maximum of 128.8 V. In Section d′–e′, the voltage ranged between 98.3 V and 128.8 V. Lastly, the voltage was ≤ 98.3 V in Section e′–f′. The ranges of the phase-to-ground voltage in the healthy Phase I are plotted in Fig. 12. In Section G–d′, the voltage ranged from 106.4 to 115 V, corresponding to the SLG fault point. Thereafter, the voltage was in the range of 112.5–129.9 V in Section d′–e′, and lastly, the voltage was ≥129.9 V in Section e′–f′.

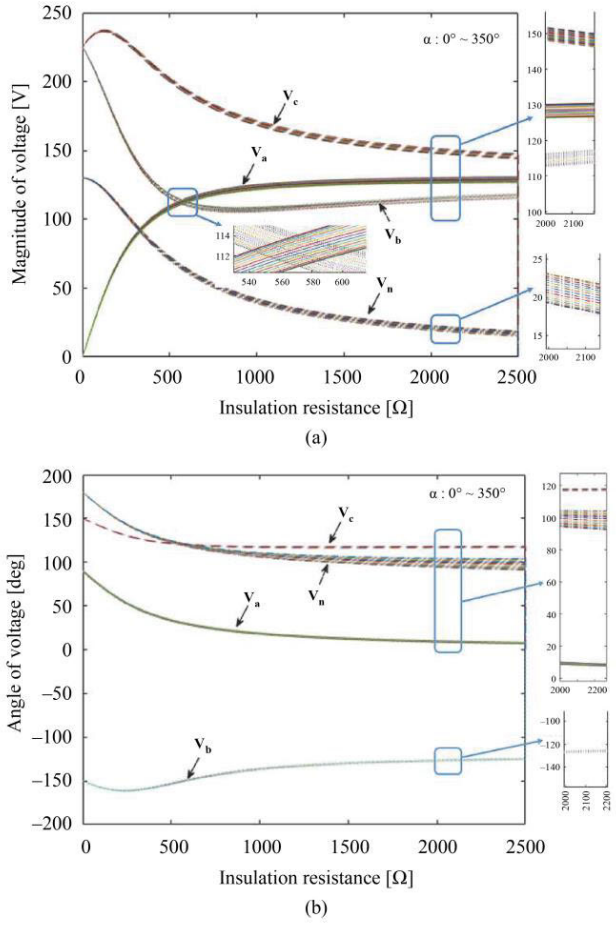


**FIGURE 9.** Variations in phase-to-ground voltage and neutral-point voltage due to phase angle change of $r_a$.

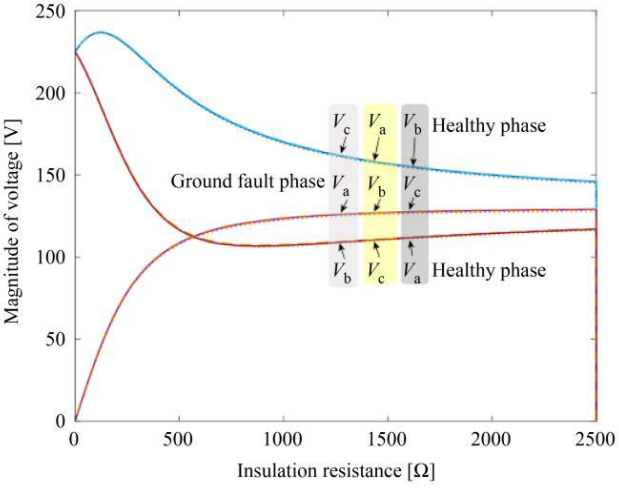


**FIGURE 10.** Variations in phase-to-ground voltage for an asymmetrical network during an arbitrary SLG fault.

The ranges of the phase-to-ground voltage in the healthy Phase II are presented in Fig. 13. In Section G–d′, the voltage

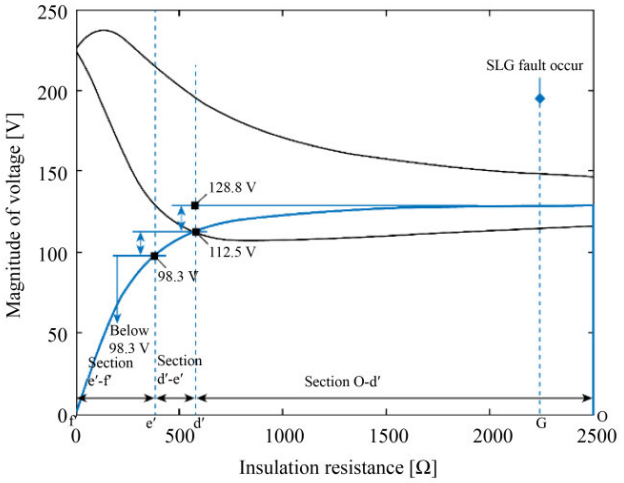


**FIGURE 11.** Ranges of the phase-to-ground voltage in faulty phase during an arbitrary SLG fault.

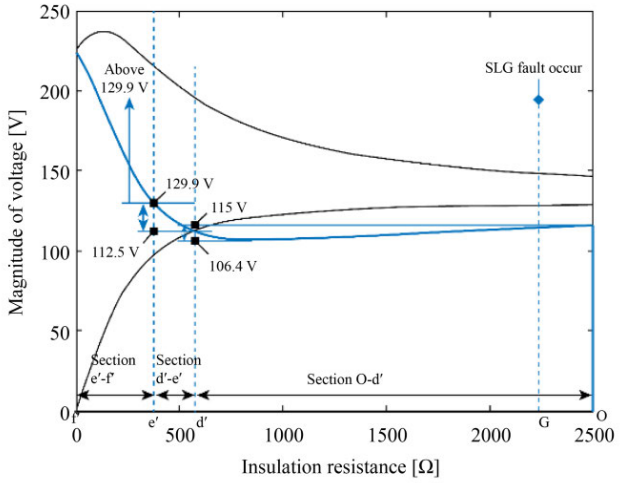


**FIGURE 12.** Ranges of the phase-to-ground voltage in healthy Phase I during an arbitrary SLG fault.

ranged between a minimum of 148.1 V (SLG fault point) and a maximum of 195.7 V, whereas the voltage was in the range 195.7–214.5 V in Section d′–e′. Furthermore, the voltage was ≥214.5 V in Section e′–f′ and attained the value of the line-to-line voltage after crossing the maximum value. Based on the analysis thus far, the ranges of the phase-to-ground voltages for the faulty and healthy phases in the three sections are summarized in Table 4.

Upon directly measuring the line-to-ground capacitance on the ship, the ground fault can be accurately determined based on the simulation conducted in this study. Therefore, we propose a practical method to determine the ground-fault phase using the directly measured phase-to-ground voltage and Table 4.

For instance, let us assume that the phase-to-ground voltages measured by a ship engineer are 111 V, 127 V, and 154 V.

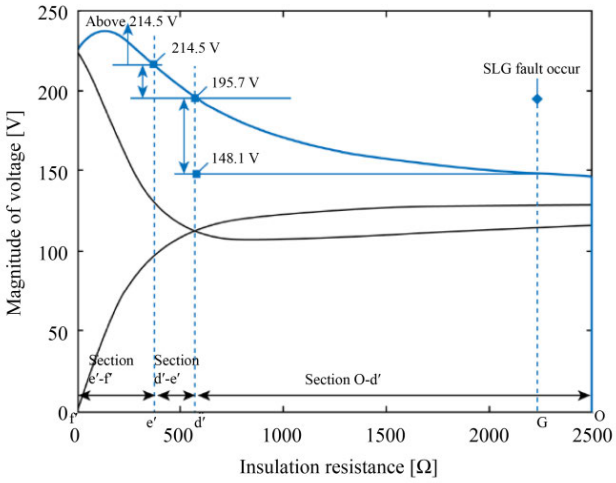


**FIGURE 13.** Ranges of the phase-to-ground voltage in healthy Phase II during an arbitrary SLG fault.

**TABLE 4.** Ranges of phase-to-ground voltage in faulty and healthy phases during an arbitrary SLG fault [unit: V].

| Section | Phase-to-ground voltage range | | |
|---|---|---|---|
| | Faulty phase | Healthy Phase I | Healthy Phase II |
| G–d′ | 112.5–128.8 | 106.4–115.0 | 148.1–195.7 |
| d′–e′ | 98.3–112.5 | 112.5–129.9 | 195.7–214.5 |
| e′–f′ | < 98.3 | > 129.9 | > 214.5 |

First, upon comparing the phase-to-ground voltages with those in Table 4, these three voltages can be associated with the first row of Table 4. Since 127 V is within the voltage range of the fault phase (112.5–128.8 V), the values 111 V and 154 V are in the voltage ranges of Healthy Phase I (106.4–115.0 V) and Healthy Phase II (148.1–195.7 V), respectively. Therefore, the phase with phase to ground voltage of 127 V can be recognized as a faulty phase.

Second, the measured voltages are 100 V, 127 V, and 212 V. These phase-to-ground voltages correspond to the values listed in the second column of Table 4 : 100 V is within the voltage range of the faulty phase (98.3–112.5 V), and 127 V and 212 V are in the voltage ranges of Healthy Phase I (112.5–129.9 V) and Healthy Phase II (195.7–214.5 V), respectively. Consequently, the phase with a phase to ground voltage of 100 V is identified as the faulty phase.

Currently, ship engineers assess the ground fault level from a permanent insulation monitor installed on the main switchboard; however, its poor sensitivity hinders the evaluation accuracy. In contrast, the proposed method can be immediately implemented in the training ship.

**TABLE 5.** Ranges of phase-to-ground voltage in faulty and healthy phases FOR arbitrary Ships[unit: V].

| Section | Phase-to-ground voltage range | | |
|---|---|---|---|
| | Faulty phase | Healthy Phase I | Healthy Phase II |
| (G–d′) x $\beta$ | (112.5–128.8) x $\alpha$ | (106.4–115.0) x $\alpha$ | (148.1–195.7) x $\alpha$ |
| (d′–e′) x $\beta$ | (98.3–112.5) x $\alpha$ | (112.5–129.9) x $\alpha$ | (195.7–214.5) x $\alpha$ |
| (e′–f′) x $\beta$ | < 98.3 x $\alpha$ | > 129.9 x $\alpha$ | > 214.5 x $\alpha$ |

### F. THE SCALABILITY TO A DIVERSE RANGE OF SHIPS

To extend the application to other low-voltage ships, it is essential to consider the rated voltage, line-to-ground capacitances, and power capacity. The relationship between these three variables and the phase-to-ground voltage is as follows.

First, the rated voltage is directly proportional to the magnitude of the phase-to-ground voltage. Specifically, if the rated voltage is doubled, the magnitude of the phase-to-ground voltage also doubles. Furthermore, the rated voltage is independent of any specific point on the insulation resistance (as observed on the x-axis of Figs. 11-13). Second, the ground capacitance is inversely proportional to any specific point on the insulation resistance. This means that if the ground capacitance is doubled, the value at point G (or d', e') in Figs. 11-13 is halved. Additionally, the ground capacitance does not affect the magnitude of the phase-to-ground voltage. Lastly, the power capacity has a negligible impact on the trend of the phase-to-ground voltage.

Assuming the rated voltage of 225 V and line-to-ground capacitance of 2.6767 $\mu$F, of the training ship "H", to be 1 p.u. (per-unit), these relationships hold true when the rated voltage is in the low-voltage range and the line-to-ground capacitance and power capacity are each in the range of 0.5 p.u. to 5 p.u.

Utilizing this information, the SLG fault diagnosis table can be adapted for any ship (with rated voltage $V_r$ and line-to-ground capacitance $C_r$). In the Table 5, $\alpha$ and $\beta$ are conversion factors, where $\alpha$ p.u. $= V_r/225$ and $\beta$ p.u. $= 2.6767/C_r$.

Thus, by knowing only the $V_r$ and $C_r$, the SLG fault can be easily diagnosed using Table 5.

This implies that the methodology presented in this study can be extended to a wide range of ships and offers ship engineers a more straightforward and convenient approach to diagnosing SLG faults compared to other approaches in the literature reviewed.

## V. CONCLUSION

Stable management of ship power systems is critical because they are operated independently of the land. Generally,

ground faults cause various problems, such as damage to cable insulation owing to increased phase-to-ground voltage.

Therefore, ship engineers should rapidly identify and manage ground faults to prevent further failures and secure the ship.

Most ships utilize ungrounded systems, and ground faults contribute to several electric faults; however, their on-site identification is challenging.

This study proposed a method for ship engineers to swiftly identify the causes of ground faults and the faulty phase. To this end, SLG faults were divided into three sections, and the variation characteristics of the phase-to-ground voltage and neutral-point voltage were analyzed.

The proposed method was applied to a three-phase, 225 V distribution network of a training ship for validation, wherein the line-to-ground capacitances were measured using an LCR meter. The measurements revealed an asymmetry ratio of 0.49% (∼0.5%), which approached the maximum asymmetry ratio for pure cable lines. Based on the measurements, the variation characteristics of the phase-to-ground voltage and neutral-point voltage were simulated using MATLAB® 2016a considering the gradual decrease in resistance at the ground fault point. Concurrently, the symmetry and asymmetry of line-to-ground capacitance were also considered.

Through this process, we proposed a comparative table enabling the convenient analysis of ground faults and their phases which was directly applicable to the training vessel "H". Therefore, engineers can recognize and identify the ground fault on ships by measuring the phase-to-ground voltages and referring to Table 4.

Nevertheless, Table 4 is tailored to specific vessels, which limits its applicability across a diverse range of ships.

To overcome this shortcoming, the relationships between phase-to-ground voltage and the three variables (rated voltage, line-to-ground capacitances, and power capacity) to be considered when extended to arbitrary ships are investigated. Based on these relationships, a generalized and practical method that can be extended to various types of ships is also proposed. Furthermore, a notable drawback is the need for engineers to procure LCR meters for measuring line-to-ground capacitance. Additionally, since this study introduces a novel approach applied directly to low-voltage ships, there exists a limitation in that it cannot be directly compared with existing methodologies.

Subsequently, we envisage conducting additional research to extend the application of the method proposed in this study to ships equipped with high voltage (3.3 kV or 6.6 kV) electrical power systems.

## REFERENCES

[1] W. Wang, L. Yan, X. Zeng, B. Fan, and J. M. Guerrero, "Principle and design of a single-phase inverter-based grounding system for neutral-to-ground voltage compensation in distribution networks," *IEEE Trans. Ind. Electron.*, vol. 64, no. 2, pp. 1204–1213, Feb. 2017, doi: 10.1109/TIE.2016.2612180.

[2] D. H. Lubich, "High resistance grounding and fault finding on three phase three wire (delta) power systems," in *Proc. IEEE Annu. Textile, Fiber Film Ind. Tech. Conf.*, Greenville, SC, USA, May 1997, pp. 10–15, doi: 10.1109/TEXCON.1997.598534.

[3] J. P. Nelson and P. K. Sen, "High-resistance grounding of low-voltage systems: A standard for the petroleum and chemical industry," *IEEE Trans. Ind. Appl.*, vol. 35, no. 4, pp. 941–948, Jul. 1999, doi: 10.1109/28.777204.

[4] J. C. Das and R. H. Osman, "Grounding of AC and DC low-voltage and medium-voltage drive systems," *IEEE Trans. Ind. Appl.*, vol. 34, no. 1, pp. 205–216, Jan. 1998, doi: 10.1109/28.658747.

[5] S.-R. Nam, S.-H. Kang, S.-J. Ahn, and J.-H. Choi, "Single line-to-ground fault location based on unsynchronized phasors in automated ungrounded distribution systems," *Electr. Power Syst. Res.*, vol. 86, pp. 151–157, May 2012, doi: 10.1016/j.epsr.2011.12.010.

[6] Y. Li, X. Meng, and X. Song, "Application of signal processing and analysis in detecting single line-to-ground (SLG) fault location in high-impedance grounded distribution network," *IET Gener., Transmiss. Distrib.*, vol. 10, no. 2, pp. 382–389, Feb. 2016, doi: 10.1049/iet-gtd.2015.0555.

[7] X. Wang, H. Zhang, F. Shi, Q. Wu, V. Terzija, W. Xie, and C. Fang, "Location of single phase to ground faults in distribution networks based on synchronous transients energy analysis," *IEEE Trans. Smart Grid*, vol. 11, no. 1, pp. 774–785, Jan. 2020, doi: 10.1109/TSG.2019.2938667.

[8] G. Song, C. Wang, T. Wang, M. Kheshti, and X. Kang, "A phase selection method for wind power integration system using phase voltage waveform correlation," *IEEE Trans. Power Del.*, vol. 32, no. 2, pp. 740–748, Apr. 2017, doi: 10.1109/TPWRD.2016.2577890.

[9] *IEEE Recommended Practice for Grounding of Industrial and Commercial Power Systems*, Standard 142-2007, 1991.

[10] J. Sottile and L. E. Holloway, "An overview of fault monitoring and diagnosis in mining equipment," *IEEE Trans. Ind. Appl.*, vol. 30, no. 5, pp. 1326–1332, Sep. 1994, doi: 10.1109/28.315247.

[11] Z. Xiangjun, K. K. Li, W. L. Chan, and Y. Xianggen, "On-site safety evaluation for Earth fault in mining power systems," *IEEE Trans. Ind. Appl.*, vol. 39, no. 6, pp. 1563–1569, Nov. 2003, doi: 10.1109/TIA.2003.818994.

[12] T. Novak and J. L. Kohler, "Technological innovations in deep coal mine power systems," *IEEE Trans. Ind. Appl.*, vol. 34, no. 1, pp. 196–204, Jan. 1998, doi: 10.1109/28.658746.

[13] X. Zeng, K. K. Li, W. L. Chan, S. Su, and Y. Wang, "Ground-fault feeder detection with fault-current and fault-resistance measurement in mine power systems," *IEEE Trans. Ind. Appl.*, vol. 44, no. 2, pp. 424–429, Mar. 2008, doi: 10.1109/TIA.2008.916744.

[14] A. Somani, B. K. Johnson, and H. L. Hess, "Evaluation of grounding and protection methods for a shipboard power system," in *Proc. IEEE Electr. Ship Technol. Symp.*, Philadelphia, PA, USA, Jul. 2005, pp. 117–124, doi: 10.1109/ESTS.2005.1524664.

[15] B. Wang, J. Geng, and X. Dong, "High-impedance fault detection based on nonlinear voltage–current characteristic profile identification," *IEEE Trans. Smart Grid*, vol. 9, no. 4, pp. 3783–3791, Jul. 2018, doi: 10.1109/TSG.2016.2642988.

[16] Y. Xue, X. Chen, H. Song, and B. Xu, "Resonance analysis and faulty feeder identification of high-impedance faults in a resonant grounding system," *IEEE Trans. Power Del.*, vol. 32, no. 3, pp. 1545–1555, Jun. 2017, doi: 10.1109/TPWRD.2016.2641045.

[17] K. Yu, Q. Yu, X. Zeng, J. Zeng, Y. Ni, H. Zou, and F. Liu, "A novel method of high impedance fault detection and fault resistance calculation based on damping rate double-ended measurement for distribution network," *Int. J. Electr. Power Energy Syst.*, vol. 136, Mar. 2022, Art. no. 107686, doi: 10.1016/j.ijepes.2021.107686.

[18] *H869 HV Power Distribution System Course*, ABB Marine Academy Singapore, Zürich, Switzerland, 2014.

[19] P. Liu and C. Huang, "Detecting single-phase-to-ground fault event and identifying faulty feeder in neutral ineffectively grounded distribution system," *IEEE Trans. Power Del.*, vol. 33, no. 5, pp. 2265–2273, Oct. 2018, doi: 10.1109/TPWRD.2017.2788047.

[20] A. Nikander and P. Järventausta, "Identification of high-impedance Earth faults in neutral isolated or compensated MV networks," *IEEE Trans. Power Del.*, vol. 32, no. 3, pp. 1187–1195, Jun. 2017, doi: 10.1109/TPWRD.2014.2346831.

[21] Z. Zhixia, L. Xiao, and P. Zailin, "Fault line detection in neutral point ineffectively grounding power system based on phase-locked loop," *IET Gener., Transmiss. Distrib.*, vol. 8, no. 2, pp. 273–280, Feb. 2014, doi: 10.1049/iet-gtd.2013.0235.

[22] Z. Jianwen, H. Hui, G. Yu, H. Yongping, G. Shuping, and L. Jianan, "Single-phase ground fault location method for distribution network based on traveling wave time-frequency characteristics," *Electr. Power Syst. Res.*, vol. 186, Sep. 2020, Art. no. 106401, doi: 10.1016/j.epsr.2020.106401.
[23] Y. Chen, J. Yin, Z. Li, and R. Wei, "Single-Line-to-Ground fault location in resonant grounded systems based on fault distortions," *IEEE Access*, vol. 9, pp. 34325–34337, 2021, doi: 10.1109/ACCESS.2021.3061211.
[24] S. Zhang, Y. Wang, M. Liu, and Z. Bao, "Data-based line trip fault prediction in power systems using LSTM networks and SVM," *IEEE Access*, vol. 6, pp. 7675–7686, 2018, doi: 10.1109/ACCESS.2017.2785763.
[25] C. Cui, W. Lin, Y. Yang, X. Kuang, and Y. Xiao, "A novel fault measure and early warning system for air compressor," *Measurement*, vol. 135, pp. 593–605, Mar. 2019, doi: 10.1016/j.measurement.2018.12.029.
[26] F. Harrou, B. Taghezouit, and Y. Sun, "Improved *k*NN-based monitoring schemes for detecting faults in PV systems," *IEEE J. Photovolt.*, vol. 9, no. 3, pp. 811–821, May 2019, doi: 10.1109/JPHOTOV.2019.2896652.
[27] B. Liu, "Analysis and application of zero-sequence voltage of single-phase ground fault asymmetrical system," *Proc. CSEE*, vol. 34, no. 28, pp. 4959–4967, 2014.
[28] J. Meng, W. Wang, X. Tang, and X. Xu, "Zero-sequence voltage trajectory analysis for unbalanced distribution networks on single-line-to-ground fault condition," *Electr. Power Syst. Res.*, vol. 161, pp. 17–25, Aug. 2018, doi: 10.1016/j.epsr.2018.03.024.
[29] J. P. Kim, "Characteristics of loci on-line-to-earth voltage according to earth fault in earthing system for ships," *J. Korea Acad. Ind. Coop. Soc.*, vol. 22, pp. 487–495, Feb. 2021, doi: 10.5762/KAIS.2021.22.2.487.
[30] P. Wang, B. Chen, C. Tian, B. Sun, M. Zhou, and J. Yuan, "A novel neutral electromagnetic hybrid flexible grounding method in distribution networks," *IEEE Trans. Power Del.*, vol. 32, no. 3, pp. 1350–1358, Jun. 2017, doi: 10.1109/TPWRD.2016.2526054.

**KI-TAK RYU** received the B.Eng. degree in marine system engineering and the M.Eng. and Ph.D. degrees in mechatronics engineering from Korea Maritime and Ocean University, Busan, South Korea, in 2001, 2008, and 2023, respectively. From March 2001 to May 2005, he was a Ship Engineer with Hyundai Merchant Marine. He joined Korea Institute of Maritime and Fisheries Technology, Busan, in May 2007, where he is currently a Full Professor. His research interests include genetic algorithms and their application, fuzzy control, and ship electric and control systems.

**YUN-HYUNG LEE** received the B.Eng. and M.Eng. degrees in marine system engineering and the Ph.D. degree in mechatronics engineering from Korea Maritime and Ocean University, Busan, South Korea, in 2002, 2004, and 2007, respectively. From February 2008 to June 2014, he was a Professor with Korea Port Training Institute, Busan. In July 2014, he joined Korea Institute of Maritime and Fisheries Technology, Busan, where he is currently a Full Professor. His research interests include genetic algorithms and their application, fuzzy control, and ship electric and control systems.